IOP Publishing Semiconductor Science and Technology
Semicond. Sci. Technol. **34** (2019) 085003 (11pp) https://doi.org/10.1088/1361-6641/ab2c21

Capacitance spectroscopy of structures with Si nanoparticles deposited onto crystalline silicon p-Si

M M Sobolev, O S Ken, O M Sreseli, D A Yavsin and S A Gurevich

Ioffe Institute, Russian Academy of Sciences, 194021 St. Petersburg, Russia

E-mail: m.sobolev@mail.ioffe.ru

Received 14 February 2019, revised 3 June 2019
Accepted for publication 24 June 2019
Published 5 July 2019

Abstract

Capacitance spectroscopy has been used to study close-packed amorphous silicon nanoparticle layers (100 nm) deposited on p-type crystalline silicon by the laser electrodispersion method. It was found that this structure is an Au-nano-Si-p-Si p–n heterojunction that exhibit rectifying properties. In addition, a plateau was observed in its capacitance–voltage ($C-V$) characteristics, which indicates that the structure has a layer with spatially localized carriers. The thickness of this layer coincides with that of the deposited layer of amorphous nanoparticles. It was found by using deep level transient spectroscopy (DLTS) to examine the carrier emission from deep traps that position and amplitudes of the DLTS peaks E1 and E3, associated with localized states, synchronously vary both with the pulse voltages U_b and filling pulse voltages U_f when illuminated with white light. These dependences a due, respectively, (1) to an increase in the population of localized states upon a change in the position of the Fermi level because of the recharging of deep defects, (2) to the Coulomb interaction of carriers localized in the deep E3 and E1 states of the nano-Si layer and in the ionized surface states of Si nanoparticles, and (3) to the Stark effect. All the above specific features of the object under study are properties of quantum-dots (QDs) in which E3 and E1 are the ground and excited states of these QDs, respectively. Finally, it was observed that levels associated with the s- and p-states have too small capture cross sections that are not characteristic of QDs. It was suggested that the significant decrease in these values may be due to the hopping conduction mechanism.

Keywords: capacitance spectroscopy, amorphous silicon nanoparticle, close-packed, spatially localized carriers, quantum-dots

(Some figures may appear in colour only in the online journal)

1. Introduction

The interest in studying the properties of silicon nanostructures is largely due to the new opportunities that open up because this material is used to create highly efficient photovoltaic solar cells (SCs) and photodiodes. A team of researchers at Kaneka Corporation have produced an array of silicon-based SCs that demonstrated a record-breaking efficiency of 26.3% [1]. The SCs were fabricated from thin crystalline silicon with corrugated surface for minimizing the reflection of light and had an amorphous silicon coating for diminishing the loss of carriers and interdigital design of electrodes. Using the achievements of nanotechnology makes it possible to significantly improve the characteristics of silicon SCs. In several studies silicon nanoparticles were used as an additional intermediate layer in a SC to raise the absorption in the short-wavelength part of the spectrum [2] and as a layer providing better utilization of the UV part of the solar spectrum via impact ionization [3]. However, the absorption of light in quasi-zero-dimensional is substantially lower than that in devices based on thin film semiconductors because of the low density of the obtained layers. One of the most promising procedures for deposition of layers of Si nanoparticles on nearly any kind of surface is the laser

electrodispersion (LED) method [4]. It is based on cascade fission of molten droplets charged in the laser-torch plasma. The method can produce ensembles of close-packed, but not coagulated Si nanoparticles (nano-Si) with small size dispersion over the ensemble [5].

Studies of the electrical properties of nano-Si layers have shown that the layers possess a relatively high conductivity comparable at 300 K with, e.g. the conductivity of crystalline Si and a carrier concentration on the order of $10^{12}\,\mathrm{cm}^{-3}$, which is an advantage as regards their application in optoelectronics. It was also shown in [5, 6] that the conductivity of the layers is nearly independent of the type and level of doping of the starting silicon target from which Si nanoparticles are produced. In [7], granular metallic films (Cu and Ni) deposited by the method of LED were examined. It was found that the particle density was such that the conductivity in these films was due to the tunneling transport of electrons (below the percolation threshold). The structure of the film was heterogeneous: particles formed aggregates consisting of several closely spaced grains. These aggregates were separated by a network of dielectric gap with width exceeding 3 nm. Because tunneling through such a gap is extremely unlikely, it is shown that, to explain the experimental results, it is necessary to invoke a model in which the variable-range hopping conduction via intermediate particles is considered. The authors of [5] measured the optical transmission and reflection spectra of granulated layers deposited in a vacuum and at various pressures of oxygen introduced into the chamber for passivating the surface of the nanoparticles. It was found that the optical constant spectra of the layers under study are correlated with the spectra of bulk amorphous silicon. However, the values obtained noticeably differ from the parameters of bulk amorphous silicon. The differences were attributed to the considerable volume of voids between the nanoparticles and to the large number of dangling bonds on their surface.

An analysis of the Raman spectrum obtained for a film of Si nanoparticles deposited on a single-crystal silicon substrate showed that [6], in addition to a narrow substrate line, the Raman spectrum has a broad and weakly structured band associated with the scattering in a layer of deposited Si particles. The violation of the translation symmetry of the crystal lattice in objects of this kind fully lifts the restriction imposed by the quasi-momentum conservation law ($q = 0$). As a consequence, phonons with any wave vectors are allowed in the Raman spectra of these samples and, in the end, reproduce the density of acoustic and optical vibrational states of crystalline silicon. The type of spectrum suggests that Si nanoparticles manufactured by the LED method are amorphous.

The optical, electrical, and photoelectric properties of heterostructures based on nano-Si layers were studied in [5, 6]. It was shown that the nano-Si layers are of n-type. In [6], the photoelectrochemical method was used to the conductivity type of semiconductors without deposition of ohmic contacts. It was shown that the nano-Si layers are *n*-type. In addition, measurements of current−voltage ($I-V$) characteristics of Au-nano-Si-p-Si structures demonstrated that these structures have rectifying $I-V$ characteristics. The forward $I-V$ characteristic followed at high biases the power law typical of the space-charge-limited current involving carrier capture levels in the energy gap, which are possibly associated with defects on the surface of nanoparticles. Under the reverse bias, the dark current linearly increased as the voltage was raised, rather than leveling-out. This indicated that the generation-recombination current in the layer of nanoparticles contributed to the reverse current of the structure.

Thus, studies of heterostructures based on close-packed amorphous nano-Si layers have revealed a number of important properties and characteristics of these structures. However, parameters of electrically active defects within a layer and on the surface of nanoparticles (dangling bonds, point defects, etc) have not been determined, and the question of whether the nanoparticles under study can be considered quantum dots (QDs) remains unanswered. At present, capacitance spectroscopy methods are among the most effective methods for studying the ground and excited QD states as well as deep-level defects in heterostructures. These are, first, the capacitance−voltage ($C-V$) spectroscopy making it possible to determine the effective carrier distribution profiles in QD structures [8] and, second, deep level transient spectroscopy (DLTS) of p−n heterostructures [9].

In this study, we continue to examine by capacitance spectroscopy [10], and analyze the temperature dependences of $I-V$ characteristics of the p−n heterostructures with layers of close-packed amorphous Si nanoparticles produced by LED. The nature of the specific features observed in the $C-V$ characteristics and DLTS spectra is discussed.

2. Experimental samples and measurement procedures

Layers (100 nm thick) of close-packed amorphous Si nanoparticles were fabricated by the LED method on p-type single-crystal Si substrates ([111]) without any special heating [4–6, 10]. The resistivity of the p-type substrate was 1 Ω cm, which corresponds to an impurity concentration of about $2 \times 10^{16}\,\mathrm{cm}^{-3}$. A silicon target (silicon wafer KDB 10 [111]) irradiated with a YAG-Nd laser ($\lambda = 1.06\ \mu$m) having a pulse duration of 30 ns and pulse energy of 0.3 J. The resulting submicrometer liquid-metal droplets were extracted from the target surface and, with a cascade division of liquid droplets charged in a laser plasma, spherical silicon particles of size 1.2 nm were formed and deposited onto the surface of the support. The amount of the deposited material and, consequently, the particle density on the support was varied by changing the deposition duration. The surface of the supporting silicon (100) single crystals was prepared by boiling in acetone and subsequent treatment with hydrogen peroxide in acidic and alkaline media, followed by washing and drying. The size of the substrate used in the study is $1 \times 1\,\mathrm{cm}^2$. The ohmic contact to the substrate was fabricated preliminarily via thermal evaporation of Al in a vacuum and the subsequent alloying. A small upper ohmic contact ($0.07\,\mathrm{mm}^2$) to a nano-Si layer was deposited by magnetron sputtering of Au. Deep-level traps and the effective carrier distribution profiles in Au-

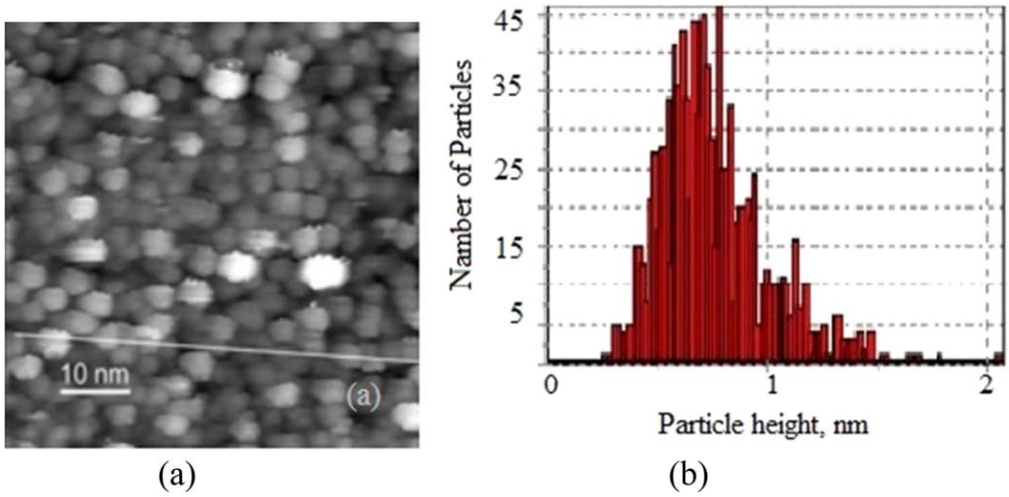

Figure 1. (a) STM image of the surface of a granulated Si film, (b) particle height distribution (the substrate is pyrolytic graphite).

nano-Si-p-Si heterostructures were studied by the DLTS and $C-V$ methods with a BIORAD DL4600 spectrometer (UK) operating in the double-strobe integration mode. The capacitance was measured with a Boonton 72B bridge at a frequency of 1 MHz. The capacitance was measured with a Boonton 72B bridge at a frequency of 1 MHz. The amplitude of the measurement signal was 15 mV, the duration of the filling pulse used in DLTS measurements was $\tau_p = 100\,\mu$s. The sensitivity of this installation is $\Delta C/C_0 \approx 10^{-4}$. To recharge traps with deep levels, the $C-V$ characteristics and the DLTS spectra were measured both in the dark and under exposure of a sample to white light. The thermal activation energy E_a of deep-level traps and their carrier-capture cross-sections $\sigma_{n,p}$ were found from Arrhenius temperature dependences.

Dark $I-V$ characteristics of the Au-nano-Si-p-Si structures were measured on a computerized setup based on ELYPOR-3 potentiostat in the temperature range from 118 to 297 K.

3. Results and discussion

The structural properties of the obtained granulated Si films were studied by scanning tunneling microscopy (STM) and atomic force microscopy (AFM) methods. For STM studies, particles were deposited on pyrolytic graphite substrates. The measurements were carried out in high vacuum after preheating the samples at 600 °C. Without preliminary hearing, the images of the samples were very noisy. Typical STM image of a structure with a degree of surface filling less than one layer of particles is shown in figure 1(a). As seen on surface histogram (figure 1(b)), the distribution of particle height lies in the range from 0.5 to 1.0 nm with a maximum of about 0.75 nm. At the same time, as follows from figure 1(a), the average particle size in the substrate plane is about 3.0 nm. This difference in size may be due to the blurring of the image in the plane due to the finite radius of curvature of the tip of the STM probe. Heated substrates were used to remove contaminants from the surface of the structure and to perform qualitative measurements. This procedure did not change the object to be analyzed. Besides, the data obtained with the STM correlate with the data obtained by means of TEM. A joint analysis of the results of STM (figure 1) and AFM (figure 2) measurements made it possible to establish that the nano-Si layer is a layer of close-packed Si nanoparticles having the shape of an ellipsoid (or hemisphere). As is well known, detecting objects less than one nanometer in size is a difficult task, there is no unambiguous method for diagnostics of nanoparticles. According to the AFM data given below (figures 2(a) and (b)), the size of nanoparticles is determined only along the height of nanoparticles. The lateral dimensions were eventually broadened when the nanoparticles were measured by STM microscopy. The average size in the substrate plane was about 1.2 nm (figure 1(b)), which is comparable with the de Broglie wavelength of an electron localized within the Si-nanoparticle. Note that on the STM images, individual Si particles could be seen well not only in rare, but also in thicker films, with a more developed profile, the thickness of which corresponds to the multilayer coating. This means that the Si nanoparticles obtained do not coagulate even when in direct contact with each other in close-packed films.

Measurements of the temperature dependences of conductivity of films of amorphous Si nanoparticles demonstrated that the conductivity of the layers is thermally activated with activation energy of about 200 meV and is associated with the hopping conduction that involves states on the surface of nanoparticles, rather than impurity states [7]. A typical experimental temperature dependence of the conductivity of a granulated Si film is shown in figure 3.

The temperature dependence of conductivity of films of amorphous Si nanoparticles was measured on specially prepared substrates. Metal contact pads with the size of $400 \times 400\,\mu m^2$ were prepared on substrates of thermally oxidized silicon by the method of lithography. The edge of the contact pad smoothly fell to the surface of thermally oxidized silicon; the nanoparticles were deposited into the

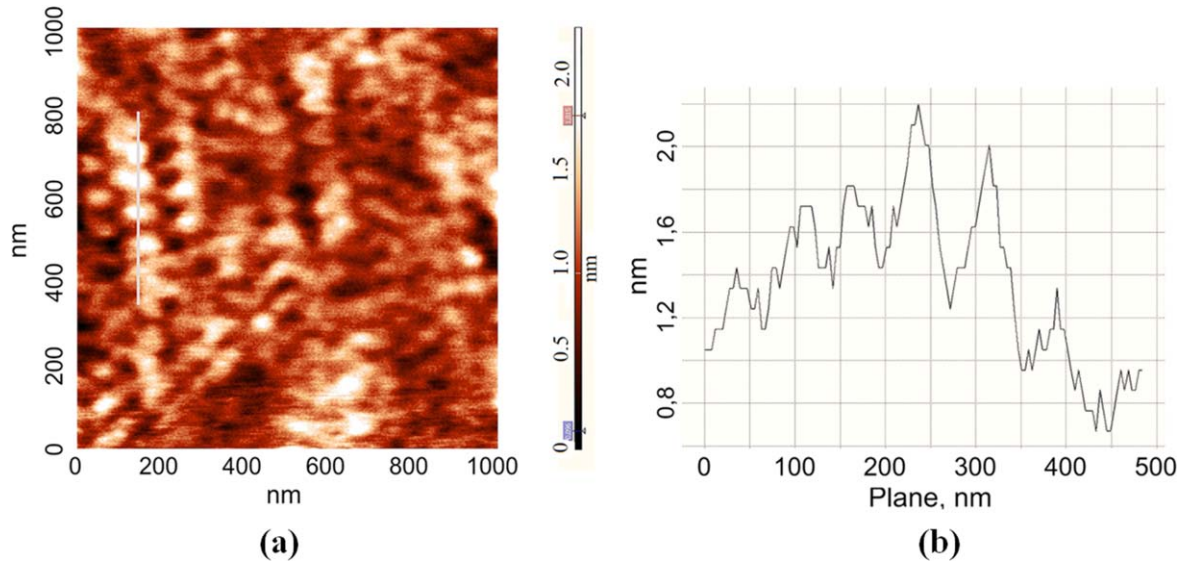

Figure 2. (a) AFM image of the surface of a granulated Si film, (b) particle height distribution along the section line (the substrate is pyrolytic graphite).

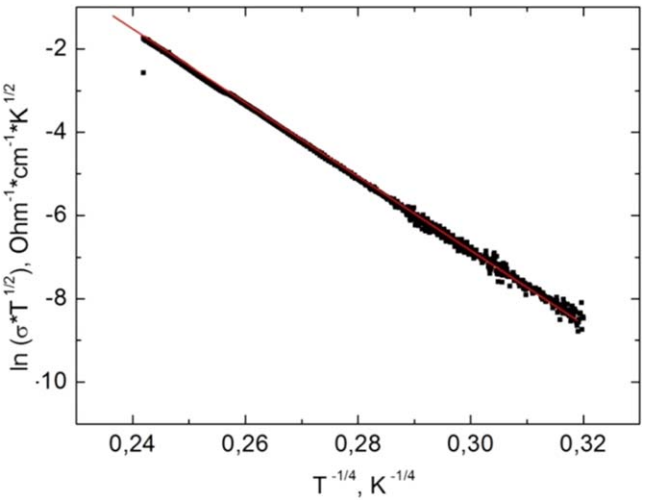

Figure 3. Temperature dependence of the conductivity of a granulated Si film. The symbol σ is the conductivity of film of amorphous Si nanoparticles.

5 μm gap between two metal pads. The temperature dependence of the conductivity of two contact structures was measured on a cryostat CCS-150 Janis Research Co. in the temperature range from 300 to 4 K. At 300 K, the resistivity of the nano-Si layer, determined from the data obtained by measuring the conductivity of the layers, is $\sim 10^3\,\Omega\,$cm in order of magnitude, which is comparable to the resistivity of single-crystal silicon with a carrier concentration of $10^{13}\,\mathrm{cm}^{-3}$.

It can be seen that this dependence is linear in the coordinates ($\ln(\sigma T^{1/2})$, $T^{-1/4}$) and, apparently, is described with good accuracy by the law proposed by Mott [11] for conductivity with variable-range hopping.

In [6], it was shown by using the photoelectrochemical method for determining the conductivity type of semiconductors without deposition of ohmic contacts that the nano-Si layers are *n*-type. In addition, measurements of current−voltage ($I-V$) characteristics of Au-nano-Si-p-Si structures demonstrated that these structures have rectifying $I-V$ characteristics. Taking into account the results of these studies, we measured the C–V characteristics of an Au-nano-Si-p-Si heterostructure. The capacitance of a p–n diode is characterized by the width (W) of the depletion layer, which depends on applied bias by the relation $W \propto (U_{\mathrm{bi}} \pm U_{\mathrm{b}})^{1/2}$, where U_{bi} is the built-in potential, and the positive and negative signs correspond to reverse and forward biases, respectively [12]. Under the forward bias, the depletion width decreases to U_{bi}, this gives rise to an increase in the depletion capacitance. At $U_{\mathrm{b}} = U_{\mathrm{bi}}$, the flat-band condition is reached due to the collapse of the depletion region, thereby diminishing the contribution of the depletion capacitance. Under the forward bias, the capacitance begins to rise upon diffusion of injected carriers. Figure 4(a) shows $C-V$ characteristics of the Au-nano-Si-p-Si heterostructure, measured under forward and reverse biases (U_{b}) in the dark and under exposure to light at room temperature. When a positive potential relative to the Au contact (forward bias) was applied to the p-Si substrate, the diffusion capacitance associated with the accumulation of minority carriers in the p-type regions was measured. At a reverse bias, a negative potential relative to the Au contact was applied to the substrate. In this case, the barrier capacitance associated with the change in of the potential barrier in the n-p junction was measured, and the width of the space-charge region (SCR) increased with growing reverse bias.

When measured under illumination, the $C-V$ characteristic had an extended plateau with a small gradient. When the characteristic was measured in the dark, the plateau became approximately twice narrower (figure 4(a)). The presence of an extended plateau in the profiles of $C-V$ characteristics is inherent in of structures containing a layer with spatial carrier

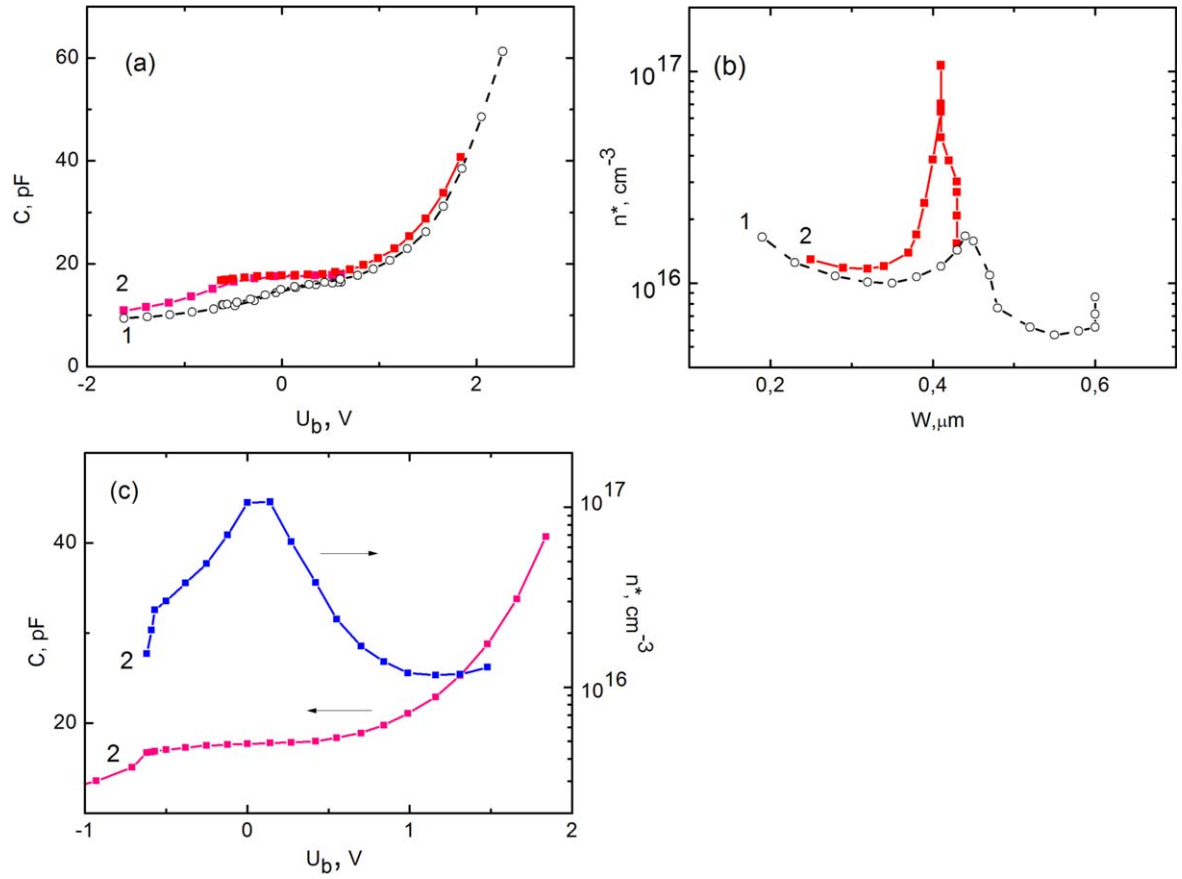

Figure 4. (a) Capacitance−voltage (C–V) characteristics, (b) distribution profiles of the effective free-carrier concentration n^* across the thickness W of the space-charge layer and (c) C–V characteristic and distribution profiles of n^* in relation to the forward and reverse bias voltages of the Au-nano-Si-p-Si heterostructures, measured at room temperature (1) in the dark and (2) under illumination.

localization (SCL), such as quantum dots and surface states, etc [13–15], and which can be attributed to release of carriers accumulated on localized states in the n-nano-Si layer is formed from close-packed and uncoagulated amorphous nanoparticles. If a structure being measured has an SCL layer, then, when the SCR with homogeneous doping merges with this layer, further penetration of the external electric field into the semiconductor will be hindered by the shielding of the field by carriers in the SCL layer. Therefore, the capacitance varies only slightly up to a voltage at which all carriers leave the SCL layer [15]. The width of the step in the $C-V$ characteristic depends on the electron concentration in the SCL layer, which, in turn, may depend on the electron occupancy of levels associated with spatially localized states at a given temperature and on the position of the Fermi level in the structure and on the applied bias voltage. At zero bias applied across the structure, the energy levels of the QDs lie below the Fermi-level of the nano-Si layer. If a reverse voltage is applied, the energy levels are raised to positions above the Fermi-level and the electrons captured in the QDs are emitted into the conduction band of nano-Si. This will raise the positive net charge in the depletion region and change the diode capacitance. From this it follows that, by changing the position of the Fermi level in the structure, it is possible to change the occupancy of spatially localized states by carriers that determine the profile of the C–V characteristic. The behavior of the C–V characteristics upon exposure to white light shows that the Au-nano-Si-p-Si heterostructure may have, in addition to spatially localized states in the nano-Si layer, defects on the surface of Si nanoparticles that are electron and hole traps on which electrons accumulate. Under exposure to white light, the position of the Fermi level may change due to the recharging of deep surface states exhibiting donor and acceptor properties, which, in turn, may change the electron occupancy of the levels related to spatially localized states in Si nanoparticles. This can occur, for example, if the concentrations of deep donors and acceptors on the surface of the Si-nanoparticles are comparable with those of shallow levels in the nano-Si layer. In this case, the concentration of uncompensated donors will decrease under optical illumination due to the recharging of deep surface states, and the Fermi level will shift closer to the conduction band [14].

Using the differential capacitance method [16], we calculated from $C-V$ characteristics the distribution profiles of the effective free electron concentration, $n^*(W)$ (figure 4(b)):

$$n^*(W) = \frac{C^3}{q\,\varepsilon\varepsilon_0\,S^2\left(\frac{dC}{dU_b}\right)},\ W = S\frac{\varepsilon\varepsilon_0}{C}, \qquad (1)$$

where ε_0 is the permittivity of free space, ε is the relative permittivity of the semiconductor, W is the SCR width, S is the area of the n–p junction, U_b is the bias voltage and q is

elementary charge. The barrier capacitance of the p–n junction is determined by equation (1), which is valid for reverse and forward bias until the diffusion capacitance is added to the barrier capacitance for the forward bias. The density measured for the nanostructured film of silicon is rather close to the density of bulk silicon, and, therefore, we use the dielectric constant of single crystal silicon in the case of the nanostructured film. Above, it was shown that the resistivities of the p-type substrate and the n-type nano-Si layer are $2 \times 10^{16}\,\mathrm{cm}^{-3}$ and $10^{13}\,\mathrm{cm}^{-3}$, respectively. From these data, it follows that the conditions for an abrupt p–n junction to be formed are satisfied, and equation (1) is valid for the structure under study. It can be seen in figures 4(b) and (c) that the $n^*(W)$ and $n^*(U_b)$ profiles have, in the case of a $C-V$ measurement under illumination, a narrow and high peak. The appearance of this peak related to emptying of localized states in the nano-Si layer. If the width of this peak is estimated in the approximation for a planar capacitor by using equation (1), it is found to coincide with the nano-Si layer thickness of ~100 nm. The SCR is situated within the nano-Si layer. In the case of measurements in the dark, the peak becomes substantially smaller, which indicates that the occupancy of levels associated with spatially localized states becomes lower. The $n^*(U_b)$ profile in figure 4(c) shows that it has a narrow and high peak at $U_b = 0$, which coincides with the middle of the extended plateau in the profiles of the C–V characteristic. As the reverse or forward bias increases within the range $U_b \approx (-0.5 \div 0.5)$ V, the width of the SCR also grows and covers the whole nano-Si layer with SCL. The $n^*(U_b)$ profile in figure 4(c) shows that it has a narrow and high peak at $U_b = 0$, which coincides with the middle of the extended plateau in the profiles of the C–V characteristic. As the reverse bias increases, the width of the SCR also increases and covers the whole nano-Si layer with SCL.

Thus, our study of $C-V$ characteristics demonstrated that, first, the whole nano-Si layer, including the heterointerface with the substrate, is a region of SCL and, second, the nano-Si layer is n-type and the Au-nano-Si-p-Si heterostructure contains a p–n junction. The last point coincides with the results of work [6].

Measurements of the $I-V$ characteristic of the heterostructure confirm the presence of a p−n junction, and those made at different temperatures (figure 5) demonstrated that the rectification factor and cutoff voltage grow with decreasing temperature, which indicates that the barrier in the structure becomes higher. The reverse current grows with increasing reverse bias, which indicates contribution of the generation-recombination current and presence of traps in the layer of nanoparticles. The reverse current decreases as the temperature is lowered, which confirms this conclusion.

The $C-V$ characteristics measured in the study made it possible to determine the voltages of the filling pulse, U_f, and bias pulse, U_b, at which signals associated with the carrier emission from the localized states of traps should be observed in DLTS spectra. The DLTS spectra in figures 6 and 7 were measured at various filling pulse voltages ($U_f = 0-0.51$ V) and various bias pulse voltages U_b, both positive and negative. With U_b varied within the range $-0.02 \div -0.8$ V

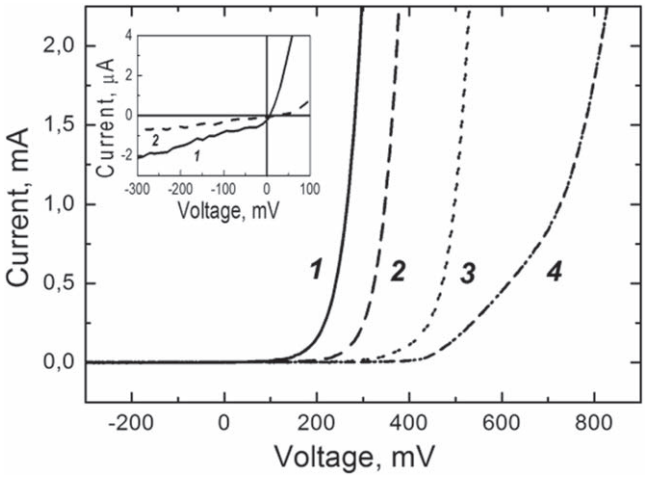

Figure 5. Current–voltage characteristics of the Au-nano-Si-p-Si heterostructure at different temperatures, K: (1) 297, (2) 267, (3) 204, (4) 119. The inset shows reverse branches of the first two curves on an enlarged scale.

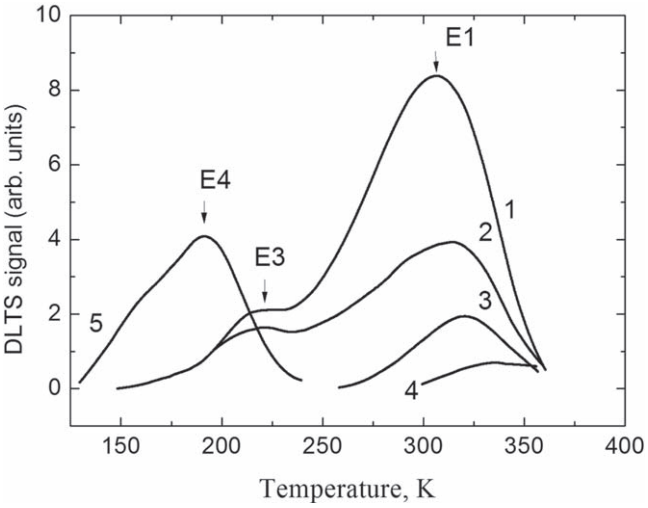

Figure 6. DLTS spectra of the Au-nano-Si-p-Si heterostructure, measured with a window rate of 200 s^{-1} at different bias pulse voltages U_b and a filling pulse voltage U_f. (1, 2, 5) at $U_f = 0.51$ V, and $U_b = -0.15$, -0.80 and 0.33 V, respectively; (3, 4) at $U_b = -0.80$ V and U_f, V: (3) 0.25, (4) 0.10 V, respectively. All the spectra were obtained in the dark.

(reverse bias), the DLTS spectra measured in the dark exhibited two broad DLTS peaks: high-temperature peak E1, the amplitude of which substantially exceeds that of the low-temperature peak E3 (figure 6, curve 1). The rather large half-widths of the peaks may be caused both by the dispersion of Si nanoparticles in the layer [3–6], and by the statistical distribution of states in amorphous a-Si. In [17], the model of size-dependent luminescence from *a*-Si:H is analyzed and it is shown that a blue shift of the luminescence energy and a general increase in the quantum efficiency of luminescence are predicted as the structure size decreases. The spectra exhibit a line width of approximately 0.13–0.14 eV, which increases to more than 0.25 eV for spheres smaller than 20 Å in diameter. By comparison, porous silicon linewidths are typically 0.3–0.4 eV. The broad, homogeneous linewidth

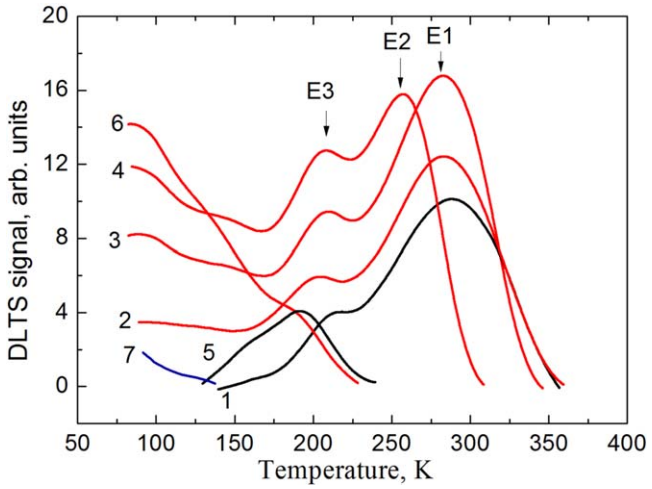

Figure 7. DLTS spectra of the Au-nano-Si-p-Si heterostructure, measured with a window rate of 200 s^{-1} filling pulse voltage $U_f = 0.51$ V and bias pulse voltages U_b, V: (1, 2) −0.13, (3) −0.02, (4) 0.14, (5, 6) 0.33; (1, 5) in the dark and (2, 3, 4, 6) under white-light illumination; (7) and U_f =0.10 V and $U_b = -0.13$ V in the dark.

predicted by this model results from the statistical distribution of states in *a*-Si:H. It also indicates that a distribution of structure sizes, which one might expect to find in nanostructured amorphous silicon, would further broaden the peak. The amplitudes of the DLTS peaks E1 and E3 decreased with increasing reverse bias pulse voltage U_b (figure 6, curve 2) and the peaks disappeared at $U_b < -1.0$ V. In addition, the amplitudes of the DLTS peaks E1 and E3 also decreased as the filling pulse voltage U_f was changed from 0.51 to 0.1 V (figure 6, curves 2−4), and the peaks disappeared at $U_f = 0$. E1 and E3 traps associated with spatially localized states do not disappear; they are not filled with electrons when the DLTS spectra are measured in the dark and at $U_f < 0$, as confirmed by the results obtained from the *C*–*V* characteristics (figure 3(a)). When the characteristic was measured in the dark, the plateau became approximately twice narrower (figure 3(a)). When $U_f < 0$, an extended plateau disappears, this indicates that there are no electrons accumulated on the n-type nano-Si layer. When the DLTS spectra are measured in the dark under $U_f = 0.1$ V and $U_b = -0.13$ V, only a low-temperature DLTS peak is observed (curve 7 in figure 6). Under optical illumination or with a filling pulse $U_f > 0$, spatially localized states are filled with electrons and peaks E1 and E3 appear in the DLTS spectra. Under the forward bias, the spectrum was constituted by only a single peak E4 (curve 5 in figure 7). Furthermore, the peaks shift to higher temperatures as U_b increases and U_f decreases. All this means that E1 and E3 peaks appearing in DLTS spectra are associated with the emission of electrons from deep traps spatially localized in the nano-Si layer adjacent to the p-Si substrate.

The fact that E1 and E3 traps are spatially localized is also confirmed by the observed rise in their DLTS amplitudes upon illumination with white light, switched on when DLTS spectra are measured (figure 7). Under illumination (curves 2, 3, 4, 6), the intensity of the DLTS spectra increases and the spectra become more complicated, with E2 peak appearing. The DLTS peaks E1 and E3 reach the highest amplitude at $U_b = -0.02$ V, which corresponds to the maximum in the distribution profile of the effective free carrier concentration, $n^*(U_b)$ (figure 4(c)).

As shown in [14, 18, 19], for the DLTS spectra of localized states the amplitude of the DLTS signal is given by expression $\Delta C/C \approx n_1 L/2N_d W$, where C is the capacitance of the space-charge layer at a pulse voltage U_b at which the DLTS signal is measured, n_1 is the surface density of electrons captured into localized states, and L is the depth at which the spatial localization layer lies, N_d is the concentration of shallow donors. Optical illumination may change the position of the Fermi level due to the recharging of deep-level defects in the nearest vicinity of these spatially localized states E1 and E3, which may favor a controlled metastable rise in their occupancy (n_1). At the same time the DLTS signal for defects distributed across the whole thickness of the semiconductor layer is determined by the relation [9] $\Delta C/C \approx N_t/2N_d$ and its amplitude grows with increasing concentration N_t of deep levels of the defect and with decreasing concentration N_d of shallow donors and is independent of illumination. Thus, the change in DLTS spectra under illumination indicates that E1 and E3 peaks are related to spatially localized states.

One more effect should be noted: in addition to the rise in the amplitude of the DLTS peaks under optical illumination, the peaks were shifted to lower temperatures, which may be due to the Coulomb interaction of localized carriers with surface states of Si nanoparticles, ionized by the illumination, or with those situated close to the interface between the nano-Si layer and the substrate [20, 21]. An electric dipole may be formed in this case between localized electrons and surface states of Si nanoparticles, ionized by the illumination. The electrostatic potential of these dipoles may lead to a change (decrease) in the height of the potential barrier for thermal emission of electrons from localized states and in the carrier capture cross-section of the dipoles, with the values of these parameters being dependent on the bias U_b and on the filling pulse voltage U_f.

The shift of E1 and E3 peaks to higher temperatures with increasing U_b in the reverse direction in the dark (curves 1 and 2 in figure 6, curves 1 in figure 7) can be accounted for by a Stark effect for deep localized states E1 and E3, i.e. by the shift of the energy levels of the localized states and by the rise in the energy of thermal emission of electrons from these states with increasing electric field strength. Under illumination (curves 2 and 3 in figure 7) the Stark effect for deep localized states E1 and E3 is also observed, but with the difference that it shifts to higher temperatures for E1 peak and to lower temperatures for E3 peak shifts. A recent experiment on Stark effect spectroscopy in InAs/GaAs self-assembled quantum dots [22] has demonstrated that a spatial separation of the electron and hole wave functions (interband built-in dipole moment) exists in the dots, which results in an asymmetric quantum-confined Stark shift in an applied electric field. The theoretical interpretation of these experimental results [23] is based on the assumption that the applied

electric field can be treated in terms of the second-order perturbation theory, which results in a quadratic dependence of the of the transition energy on the applied electric field. A nonzero dipole moment is confirmed to exist in the dots because of the asymmetric Stark shift about the zero electric field [22, 23]. The shift of the peaks of E1 and E3, observed when we measured the DLTS spectra in the dark and under illumination, is apparently due to the manifestation of an asymmetrical quantum-confined Stark shift relative to the zero electric field.

An increase in the filling pulse voltage U_f from 0.10 to 0.51 V at the pulse voltage $U_b = -0.80$ V resulted in increase of the amplitudes of the DLTS peaks E1 and E3 (figure 6), which is presumably due to the higher occupancy of the localized states. The shift of the DLTS peaks E1 and E3 to lower temperatures, observed in this case, may be due both to the increase in the occupancy of the localized states [14, 19] and to the Coulomb repulsion between electrons, which can reduce the electron capture cross-sections [18].

For a forward-biased junction ($U_b = 0.33$ V) with a narrower space-charge layer, E1 peak disappears and a new low-temperature peak E4 is observed in the dark (curve 5, figures 6 and 7), with its amplitude being approximately twice larger than that of E3 peak measured for reverse bias $U_b = -0.13$ V. When DLTS spectra are measured under illumination under the same bias at temperatures in the range from 80 to 170 K, weakly modulated bands are observed (curve 6 in figure 7). The amplitudes of these bands grow as the SCR becomes narrower, which may indicate that these bands are associated with surface states, the occupancy of which grows under illumination.

Under illumination and a low forward bias ($U_b = 0.14$ V), a new peak E2 appears in the spectrum. This peak lies on the temperature scale between peaks E1 and E3 and has amplitude close to that of E1 peak (figure 7, curve 4). This peak is of the same nature as E1 peak and its shift to the low-temperature part of the DLTS spectrum is presumably due to the manifestation of field effects.

Using the results of the DLTS spectroscopy of the Au-nano-Si-p-Si heterostructure, we determined the Arrhenius temperature dependences of the rate at which electrons are thermally emitted from localized deep traps E1, E2, and E3 and E4 (figure 8). The carrier emission rate is determined in this case by the relation [18]:

$$e_n, p = A\sigma_n, pT^2 \exp(-E_a/kT), \quad (2)$$

where A is a temperature-independent constant, and k is the Boltzmann constant. The slope ratio of the Arrhenius plot in the semilog scale was used to evaluate the energies E_a of thermal activation of electrons from the localized deep traps E1, E2, E3 and E4 observed in the DLTS spectra, and the pre-exponential factor, to find the electron capture cross-sections σ_n (figure 8, table 1).

We demonstrated that the nano-Si layer has n-type conductivity and the changes observed in the DLTS spectra, depending on the illumination and the filling pulse, are associated with the traps for majority, rather than minority carriers. These electron traps, as we assume, are related to

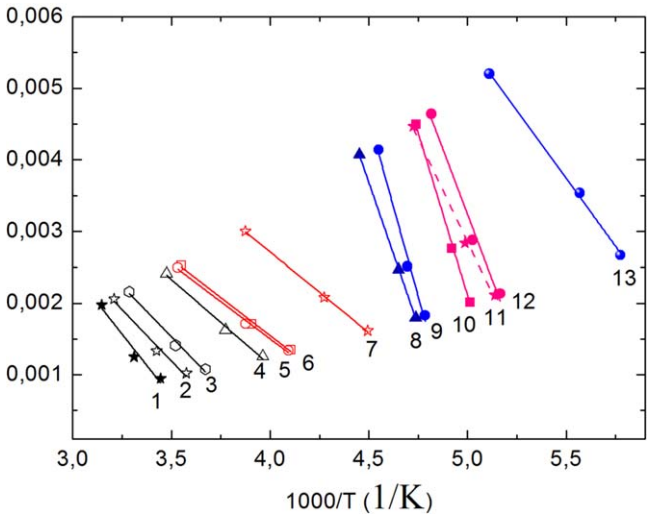

Figure 8. Arrhenius temperature dependences of the thermal emission rates e of electrons from localized deep traps E1, E2, and E3 and E4 in of the Au-n-nano-Si-p-Si heterostructure. (E1) (1) $U_f = 0.25$ V and $U_b = -0.80$ V; $U_f = 0.51$ V and U_b, V: (2) −0.80, (3) −0.15, (4) −0.13 in the dark and (5) −0.13, (6) −0.02 under white-light illumination; (E2) (7) $U_f = 0.51$ V and $U_b = 0.14$ V under white-light illumination; (E3) $U_f = 0.51$ V and U_b, V: (8) −0.15, (9) −0.13, (13) 0.33 in the dark and (10) −0.02, (11) 0.14, (12) −0.13 under white-light illumination.

spatially localized states of quantum dots. It is well known that, for distributed traps in the DLTS spectra, the majority carrier traps give a negative DLTS signal, and minority carrier traps, a positive DLTS signal. For quantum dots that are situated in an n-type matrix and have ground and excited states, everything is the opposite in measurements of DLTS spectra: when a reverse bias is applied to a sample, the quantum states are empty and the capacitance decreases. After a pulse of majority carriers is applied, the boundary of the space charge layer is shifted towards the p-type layer and majority carriers are captured by states in quantum dots, so that the capacity increases. Thus, the quantum states of main carriers give a positive DLTS signal. Another explanation of the results obtained is possible, suggesting that the nano-Si layer is p-type and the changes in the DLTS spectra, depending on the illumination and the filling pulse, are associated with traps for minority carriers (holes). It is assumed that an analysis as a function of the filling pulse duration can discriminate between the DLTS signal of point defects and the DLTS signal due to spatially localized traps, such as traps related to extended defects. However, both spatially localized states and extended defect states are distributed states, and the emission of electrons from these differs from the emission of a single energy level of a point defect. In [24], the authors discovered, in a study of defects with deep levels in GeSe/Si heterostructures with dislocations by the DLTS method, the presence of an extended defect characterized by a broadened DLTS peak. The full width at half maximum of the DLTS peak and the temperature of the DLTS peak, both decreased monotonically was the fill pulse became shorter. They attributed this behavior to the presence of a dislocation-related distribution of energy levels within the

Table 1. Electron trap levels detected from DLTS spectra.

Localized deep traps	Activation energy E_a, meV	Capture cross-section σ, cm^2	Measurement conditions		
			U_f, V	U_b, V	
E1	96	1.85×10^{-23}	0.51	−0.02	Under illumination
	95	1.75×10^{-23}		−0.13	Under illumination
	115	3.52×10^{-23}			In the dark
	156	1.75×10^{-22}		−0.15	In the dark
	165	1.37×10^{-22}		−0.80	In the dark
	208	5.50×10^{-22}	0.25		In the dark
E2	85	1.15×10^{-23}	0.51	0.14	Under illumination
E3	150	2.41×10^{-21}	0.51	0.14	Under illumination
	229	1.85×10^{-20}	0.51	−0.02	Under illumination
	193	3.08×10^{-20}		−0.13	Under illumination
	299	4.11×10^{-18}			In the dark
	314	8.06×10^{-18}		−0.15	In the dark
E4	85	1.15×10^{-22}	0.51	0.33	In the dark

GeSi band gap and to the resulting fill-pulse-dependent local band bending. Earlier, we have observed in our DLTS measurements of InGaAs/GaAs heterostructures a dependence of the thermal activation energy and capture cross-section of the acceptor-type dislocation traps on the filling pulse [25]. This dependence may be associated with the existence of an energy band in the energy gap. The possibility that a band of this kind may exist was noted in [26, 27], where it was suggested to consider a dislocation as a 1D crystal. In [25], the authors studying localized states at misfit dislocations in InGaAs/GaAs heterostructures by the method based on the optical recharging to reveal spatially localized deep interfacial states. Imagine the grounds that allow us to state that the nano-Si layer has n-type conductivity and the deep traps we observe are not related to extended defects, but are spatially localized states. *C–V* characteristic measurements revealed that the nano-Si layer has n-type conductivity. When the *C–V* characteristic was measured, this layer showed that it has an extended plateau formed due to the presence in the nano-Si layer of spatially localized states on which electrons accumulate. The nano-Si layer is formed from close-packed and uncoagulated amorphous nanoparticles. Each isolated Si nanoparticle has spatially localized states. The hopping electron transport in monodisperse granular Si was observed in the films under study of amorphous Si nanoparticles. A significant distinctive feature of spatially localized states is the manifestation of the quantum-confined Stark effect and the built-in dipole moment, the Coulomb interaction of carriers localized in deep E1 and E3 states of the nano-Si layer, and the ionized surface states of the Si nanoparticle. These effects were discovered in our study. Thus, the formation of traps related to extended defects is impossible in the nano-Si layer and they cannot be detected there. The DLTS signal was not analyzed as a function of the filling pulse duration.

Studies by STM (figure 1) and AFM (figure 2) allowed us to conclude that the nano-Si layer is spatially confined and is formed by close-packed Si nanoparticles with an average size of 2 nm, which is comparable with the de Broglie wavelength of an electron localized within a Si-nanoparticle. That is, one of the conditions for the quantum-confinement effect to be manifested in Si-nanoparticles is satisfied. However, this is not sufficient for a particle to exhibit the properties of a QD. For QDs, there must appear, as a result of the quantum confinement [28] of the motion of electron within a space smaller than the Bohr radius, with discrete ground and degenerate excited quantum states similar to s- and p-states. The number of electrons that can occupy a degenerate p-state should be at least 2 times that in the s-state [29].

When measuring $C-V$ characteristics, DLTS spectra, and STM/AFM image of the surface of a granulated Si film, we found the characteristics and properties that make it possible to consider the close-packed Si nanoparticles to be QDs. First, the Au-nano-Si-p-Si heterostructure contains a p–n junction and an n-type nano-Si layer. Second, the $C-V$ characteristic has an extended plateau that is typical of structures containing a layer with spatial localization of carriers (figure 4(a)). The width of this layer coincides with the thickness of the nano-Si layer, and a narrow distribution profile of the effective free carrier concentration, $n^*(U_b)$ (figure 4(b)), is associated with the release of electrons accumulated on localized states in the nano-Si layer. Third, two states, E1 and E3, are found in the SCL layer in a study of DLTS spectra. The position and amplitude of these states synchronously vary with U_b and U_f. The energies of these states strongly depend on the strength of the applied external field, with the quantum-confined Stark effect demonstrated. Fourth, it was found that the thermal activation energy of carriers and the amplitudes of the DLTS peaks E1 and E3 depend on the presence of illumination. The first of these dependences is associated with the Coulomb interaction of carriers localized in deep states E1 and E3 of the nano-Si layer and ionized surface states of a Si nanoparticle. The second is due to the increase in the occupancy of localized states upon a change in the Fermi level position as a result of recharging of the deep-level defects. Effects of this kind have been observed previously for QD systems produced by molecular-beam and vapor-phase epitaxy with self-organized growth of InGaAs/GaAs heterostructures [14, 19, 20]. All the above specific features of the object under study are

properties of QDs in which E3 and E1 are the ground and excited states of these QDs, respectively, with the amplitudes of the DLTS peaks differing by approximately a factor of 2. In this case, the energy of thermal activation of electrons from E3 level by ~100 meV exceeds the similar value for E1 level. This value is in agreement with the theoretical calculations of the transition energies between the lowest electron levels in the 2 nm size Si nanocrystals with SiO_2 barriers [30]. It is known that amorphous silicon nanoparticles exhibit photoluminescence and its spectral position scales with the size of the nanoparticle [30–32].

It remains unclear why the E3 and E1 levels have such a small capture cross-section. This is very astonishing for a trap level related to a QD level. There are at least two reasons why the capture cross-section may be small. First, it is not a direct capture of carriers by a QD, but involves structural defects [33]. The carrier trapping occurs in this case by the electron-phonon mechanism, which leads to a significant decrease in the carrier capture cross-section on the QD levels. Second, it is the hopping mechanism of conductivity via intermediate particles that can be operative in close-packed layers of nanoparticles [7].

4. Conclusions

We applied capacitance spectroscopy to study the spatial and quantum confinement of close-packed amorphous Si nanoparticles formed by the LED method on a p-type single-crystal Si substrate. Measurements of *C–V* characteristics showed that the p–n-Au-nano-Si-p-Si heterostructure has a layer of spatially localized carriers with thickness (100 nm) coinciding with that of the amorphous nanoparticles. The behavior of DLTS spectra measured in the dark and under white-light illumination at various pulse voltages U_b and filling pulse voltages U_f suggests that the spatially localized amorphous Si nanoparticles have an average size in the substrate plane of about 1.2 nm, which is comparable with the de Broglie electron wavelength and is smaller than the Bohr radius, and are characterized by quantum-confinement. This results in that ground and degenerate excited QD states are formed, being similar to the s- and p-states exhibiting Stark effect, electric dipole effect, and controlled metastable occupancy under optical illumination. The energies E_a of thermal activation of electrons from levels associated with quantum states and the electron capture cross-sections were determined at various bias voltages applied to the structure. An analysis of the Arrhenius temperature dependences showed that levels associated with the s- and p-states have too small capture cross sections that are not characteristic of QDs. It was suggested that these values may be due to the hopping conduction mechanism via intermediate particles, which can be operative in densely close-packed layers of nanoparticles.

Acknowledgments

The authors would like to thank V I Kozub for valuable discussions.

ORCID iDs

M M Sobolev https://orcid.org/0000-0001-9792-8689
O S Ken https://orcid.org/0000-0003-1541-863X
D A Yavsin https://orcid.org/0000-0001-6934-0407

References

[1] Yoshikawa K *et al* 2017 Silicon heterojunction solar cell with interdigitated back contacts for a photoconversion efficiency over 26% *Nat. Energy* **2** 17032–8
[2] Martí A, López N, Antolín E, Cánovas E, Stanley C, Farmer C, Cuadra L and Luque A 2006 Novel semiconductor solar cell structures: the quantum dot intermediate band solar cell *Thin Solid Films* **511–512** 638–44
[3] Sreseli O M, El'tsina O S, Belyakov L V and Goryachev D N 2009 Observation of space-separated multiexciton generation in photocurrent of Au/por-Si/p-Si structure *Appl. Phys. Lett.* **95** 031914
[4] Kozhevin V M, Yavsin D A, Kouznetsov V M, Busov V M, Mikushkin V M, Yu N S, Gurevich S A and Kolobov A 2000 Granulated metal nanostructure deposited by laser ablation accompanied by cascade drop fission *J. Vac. Sci. Technol.* B **18** 1402–5
[5] Yeltsina O S, Andronikov D A, Yu S M, Yavsin D A, Vainshtein J S, Sreseli O M and Gurevich S A 2013 Optical constants of silicon nanoparticle thin films grown by laser electrodispersion *Semiconductors* **47** 1367–71
[6] Ken O S, Andronikov D A, Yavsin D A, Kukin A V, Danilov S N, Smirnov A N, Sreseli O M and Gurevich S A 2014 Spectral features of the photoresponse of structures with silicon nanoparticles *Semiconductors* **48** 1518–24
[7] Kozub V I, Kozhevin V M, Yavsin D A and Gurevich S A 2005 Electron transport in monodisperse metal nanostructures *JETP Lett.* **81** 226–30
[8] Brounkov P N, Benyattou T and Guillot G 1996 Simulation of the capacitance–voltage characteristics of a single-quantum-well structure based on the self-consistent solution of the Schrödinger and Poisson equations *J. Appl. Phys.* **80** 864–71
[9] Lang D V 1974 Deep-level transient spectroscopy: a new method to characterize traps in semiconductors *J. Appl. Phys.* **45** 3023–32
[10] Sobolev M M, Ken O S, Sreseli O M, Yavsin D A and Gurevich S A 2018 Spatial and quantum confinement of Si nanoparticles deposited by laser electrodispersion onto crystalline Si *Tech. Phys. Lett.* **44** 287–90
[11] Mott N F and Davis E A 1971 *Electronic Processes in Non-Cristalline Materials* (Oxford: Clarendon)
[12] Sze S M 1981 *Physics of Semiconductor Devices* 2nd edn (New York: Wiley-Interscience)
[13] Brounkov P N, Konnikov S G, Ustinov V M, Zhukov A E, Yu E A, Maximov V M, Ledentsov N N and Kop'ev P S 1996 Capacitance spectroscopy of electron energy levels in InAs quantum dots in a GaAs matrix *Semiconductors* **30** 924–32
[14] Sobolev M M, Kovsh A R, Ustinov V M, Egorov A Y, Zhukov A E and Musikhin Y G 1999 Capacitance spectroscopy of deep states in InAs/GaAs quantum dot heterostructures *Semiconductors* **33** 157–64

[15] Ya A V, Demidov E V, Zvonkov B N, Murel A V and Romanov Y A 1991 Investigation of quantum wells by the method of capacitance-voltage characteristics *Sov. Phys. Semicond.* **25** 631

[16] Thomas C O, Kahng D and Manz R C 1962 Impurity distribution in epitaxial silicon films *J. Elecrochem. Soc.* **109** 1055–61

[17] Estes M J and Moddel G 1996 Luminescence from amorphous silicon nanostructures *Phys. Rev.* B **54** 14633–42

[18] Anand S, Carlsson N, Pistol M-E, Samuelson L and Seifert W 1995 Deep level transient spectroscopy of InP quantum dot *Appl. Phys. Lett.* **67** 3016–8

[19] Sobolev M M, Kovsh A R, Ustinov V M, Egorov A Y, Zhukov A E and Musikhin Y G 1999 Metastable population of self-organized InAs/GaAs quantum dots *J. Electron. Mater.* **28** 491–5

[20] Sobolev M M, Kovsh A R, Ustinov V M, Egorov A Y, Zhukov A E, Maximov M V and Ledentsov N N 1997 Deep-level transient spectroscopy in InAs/GaAs laser structures with vertically coupled quantum dots *Semiconductors* **31** 1074–9

[21] Sobolev M M and Lantratov V M 2001 The influence of Coulomb effects on the electron emission and capture in InGaAs/GaAs self-assembled quantum dots *Physica* B **308-310** 1113–6

[22] Jin P, Li C M, Zhang Z Y, Liu F Q, Chen Y H, Ye X L, Xu B and Wang Z G 2004 Quantum-confined Stark effect and built-in dipole moment in self-assembled InAs/GaAs quantum dots *Appl. Phys. Lett.* **85** 2791–3

[23] Sheng W and Leburton J-P 2002 Anomalous quantum confined Stark effects in stacked InAs/GaAs self-assembled quantum dots *Phys. Rev. Lett.* **88** 167401–4

[24] Grillot P N, Ringel S A, Fitzgerald E A, Watson G P and Xie Y H 1995 Electron trapping kinetics at dislocations in relaxed $Ge_{0.3}Si_{0.7}$/Si heterostructures *J. Appl. Phys.* **77** 3248–56

[25] Sobolev M M, Soldatenkov F Y and Shul'pina I L 2018 Misfit dislocation-related deep levels in InGaAs/GaAs and GaAsSb/GaAs p–i–n heterostructures and the effect of these on the relaxation time of nonequilibrium carriers *J. Appl. Phys.* **123** 161588

[26] Kveder V, Kittler M and Schröter W 2001 Recombination activity of contaminated dislocations in silicon: a model describing electron-beam-induced current contrast behavior *Phys. Rev.* B **63** 115208–11

[27] Gelczuk Ł, Dąbrowska-Szata M, Jóźwiak G and Radziewicz D 2007 Electronic states at misfit dislocations in partially relaxed InGaAs/GaAs heterostructures *Physica* B **388** 195–9

[28] Yu P Y and Cardona M 2010 *Fundamentals of Semiconductors: Physics and Materials Properties* 4th edn (Heidelberg: Springer)

[29] Cockins L, Miyahara Y, Bennett S D, Clerk A A, Studenikin S, Poole P, Sachrajda A and Grutter P 2010 Energy levels of few-electron quantum dots imaged and characterized by atomic force microscopy *Proc. Natl Acad. Sci.* **107** 9496–501

[30] Moskalenko A S, Berakdar J, Poddubny A N, Prokofiev A A, Yassievich I N and Goupalov S V 2012 Multiphonon relaxation of moderately excited carriers in Si/SiO_2 nanocrystals *Phys. Rev.* B **85** 85432

[31] Park N-M, Choi C-J, Seong T-Y and Park S-J 2001 Quantum confinement in amorphous silicon quantum dots embedded in silicon nitride *Phys. Rev. Lett.* **86** 1355–7

[32] Nishio K, Kōga J, Yamaguchi T and Yonezawa F 2003 Theoretical study of light-emission properties of amorphous silicon quantum dots *Phys. Rev.* B **67** 195304

[33] Bloshkin A A, Yakimov A I, Timofeev V A and Dvurechenskii A V 2014 On the process of Hole trapping in Ge/Si heterostructures with Ge quantum dots *Semiconductors* **48** 1036–40